

Observing a group to infer individual characteristics

Arshed Nabeel* and Danny Raj M†

Department of Chemical Engineering,
Indian Institute of Science, Bangalore

(Dated: October 13, 2021)

In the study of collective motion, it is common practice to collect movement information at the level of the group to infer the characteristics of the individual agents and their interactions. However, it is not clear whether one can always correctly infer individual characteristics from movement data of the collective. We investigate this question in the context of a composite crowd with two groups of agents, each with its own desired direction of motion. A simple observer attempts to classify an agent into its group based on its movement information. However, collective effects such as collisions, entrainment of agents, formation of lanes and clusters, etc. render the classification problem non-trivial, and lead to misclassifications. Based on our understanding of these effects, we propose a new observer algorithm that infers, based only on observed movement information, how the local neighborhood aids or hinders agent movement. Unlike a traditional supervised learning approach, this algorithm is based on physical insights and scaling arguments, and does not rely on training-data. This new observer improves classification performance and is able to differentiate agents belonging to different groups even when their motion is identical. Data-agnostic approaches like this have relevance to a large class of real-world problems where clean, labeled data is difficult to obtain, and is a step towards hybrid approaches that integrate both data and domain knowledge.

With the advent of sophisticated imaging techniques and machine learning algorithms, many experimental studies in the field of complex systems and complex flows turn to computer vision to investigate the underlying dynamics of the individuals (agents). Examples include the study of the motion of an intruder and the flow of grains in granular flows [1], hydrodynamics of droplet interactions in a microchannel [2], dynamics of traffic flows [3] and crowds [4], and schooling and swarming behavior of organisms such as fish [5]. In most of these examples, a camera can be setup for imaging: high-speed if the time scales of the processes are milliseconds or smaller, under a microscope if the length scales involved are of the order of microns or even use a stereo-pair of images to resolve 3D structures [6]. The agents that make up the complex system are tracked and their velocities are computed from the measurements. The motion of these agents is a result of both self-propulsion (or due to external driving) and interactions between the agents. General interest is to infer the characteristics of the agents and the underlying interactions from the observations made of the collective [7–11].

However, the fundamental question of whether it is even possible to accurately infer the ‘true’ properties of individuals from measurements, still needs to be resolved. Depending on the context of the problem, inaccuracy in identification could prove to be detrimental. For instance, consider the case of dense pedestrian crowds—e.g. in a pilgrimage site or a crowded crosswalk—where individuals may be forced in the direction of their neighbors even when they are unwilling or unable to move in that direction. Can an observer (i.e. a combination of sensors,

computer vision, estimator, etc.) that is continuously collecting and processing information of the movement of people in a crowd, predict the onset of a stampede (local or global)? In this article, we explore this question and investigate how the collective dynamics of the crowd affects an observer’s ability to infer the underlying behavior of the agents, from measurements at the level of a collective.

A crowd consisting of different groups of agents is called a *composite crowd*. Our objective is to classify the agents as belonging to one group or another based on the information of their movement. In the context of dense-crowds in pilgrimage sites discussed previously, agents could essentially belong to two categories: *Group 1* where agents move in their desired direction and *Group 2* which consists of agents that either want to change their direction or speed, or simply stop moving. As the agents are differentiated solely based on the speed (or velocity) of desired motion, one can use a simpler and more-widely studied conceptualization of a composite crowd to study this problem [12–20]; where the two groups of agents desire to move in opposite directions with the same speed.

A composite crowd of oppositely moving agents exhibit spontaneous laning phenomena where agents of the same type occupy a common lane oriented in the desired direction for movement. Once lanes are formed, agents can move freely, as they do not encounter those of the oppositely moving type. This feature is observed in a number of systems that include pedestrian movement in a crossing or a foot bridge—where people rapidly and spontaneously group with others who are going the same direction [21, 22], and oppositely charged colloids or driven complex plasmas—where laned arrangements are formed under externally imposed force fields [23, 24]. From the perspective of classifying agents, it may be easier to do so when agents occupy distinct lanes. However, it takes

* arshed@iisc.ac.in

† dannym@iisc.ac.in

time for lanes to be formed and when crowd densities are high, lane formation is not guaranteed, during which it is unclear if agents can be classified accurately. In some model systems where agents are polar and experience a torque that makes them turn in order to avoid collisions, they can exhibit a phase transition to a state where lanes are never formed called, the critically mingled state [17]. Or oppositely moving agents experiencing high thermal fluctuations (or Brownian activity to mimic panic in pedestrian crowds), lead to the formation of a jammed state resulting in dynamic freezing due to heating [25].

The classification problem becomes particularly challenging when clean, labeled data is not readily available—as is often the case for problems in real-world crowd dynamics. In these situations, we cannot rely on the traditional supervised learning techniques [26] for classification. A physics-informed approach, based on phenomenological understanding of the crowd dynamics, is appealing in this context. By incorporating insights about the dynamics, such an approach can reduce the dependence on labeled data.

In this article, we use the bi-disperse crowd with two groups of agent, each with its own desired direction of motion. We investigate how well can an observer—collecting information of the how the agents move—classify agents according to their desired direction. It is reasonable to expect that information that aids the classification of a particular agent is encoded in the motion of that agent itself. Therefore, we first examine the performance of a simple observer that takes into account only the dynamics of a focal agent. However, since the dynamics of an agent is also driven by collective effects arising from interactions with other agents, this approach often produces misclassifications. To address this, we build an improved observer that explicitly accounts for collective effects on the movement of an individual. By using a *neighborhood parameter* to quantify the influence of neighboring agents, the new observer can decouple an agent’s intrinsic motion from the motion caused by interactions with other agents. We conclude by discussing the limitations of the approach and discussing our outlook about applying such approaches to real crowds.

RESULTS

A simple model of crowd dynamics

We use a simple model of bi-disperse crowds (i.e. consisting of two distinct groups of agents), similar to the models previously used in literature [19, 25]. Agents are arranged in a 2D periodic domain, with a packing density ρ . Each agent has a desired direction of movement, which is same for all agents in the group but different between the groups (which we call Group 1 and Group 2). Group 1 agents have a desired velocity along the positive x -direction and Group 2 agents in the negative

x -direction. An agent is driven by two forces: a *restitution force*, denoting the intrinsic effort by the agent to move in the desired direction, and an *inter-agent force*, denoting the interactions between agents. The forces are designed such that the agents cannot overlap. For mathematical details of the model, see appendix A. We study how the model dynamics change with respect to two key aspects of the crowd: the relative sizes of the two groups, quantified by a *number-ratio* N_r (the fraction of agents in the minority groups), and the effort by the agents to move in their desired directions, quantified by the *intrinsic velocity* s_0 .

In the absence of any obstacles or collisions, an agent approaches its steady-state velocity $\mathbf{v}_{0,i}$ with a timescale τ . However, when there are other agents present, the inter-agent interactions affect the movement in interesting ways. An agent can be blocked or pushed around by other agents in its path, which can result in diverse dynamics depending on the model parameters.

When the packing density ρ is not too high (agents can freely move past each other), lateral migration due to interactions with other agents causes agents of the same group to find each other passively and form clusters (Figure 1(a), top panel). The cluster of agents moves together as a unit, and collisions with the opposite group appear only at its boundary. For these reasons, clustered state is an absorbing state: i.e., once a cluster is formed, it does not break easily, but new agents can join the cluster. Clustering improves mobility of the agents, as the cluster as a whole is able to better force its way through opposing agents.

When N_r is close to $\frac{1}{2}$ (symmetric or nearly symmetric regime), clustering can eventually lead to formation of system-spanning lanes (Figure 1(b), middle panel). Since each lane consists only of one group of agents, mobility is maximum (agent speeds are close to $\pm s_0$) in the laned state.

When ρ is high and the intrinsic velocity s_0 is relatively small, the crowd can enter a jammed state, where agents meet head-on and do not have enough space to move past each other (Figure 1(a), bottom panel). For the symmetric case ($N_r = \frac{1}{2}$), this causes the entire assembly to freeze. For asymmetric cases ($N_r < \frac{1}{2}$), due to an imbalance in the net force, the jammed assembly of agents slowly drifts in the direction dictated by the majority group. (See Movie S1, appendix F for an animated visualization of these cases.)

Observing agents with a simple observer model

The goal of the observer is to observe the dynamics of the system (velocities and positions of the agents), and make inferences about the agent properties—in our case, their respective group memberships (Figure 1(b)). In other words, the observer has to infer the desired directions of motion for the agents, based on the observed motion of the collective. We start with a simple observer

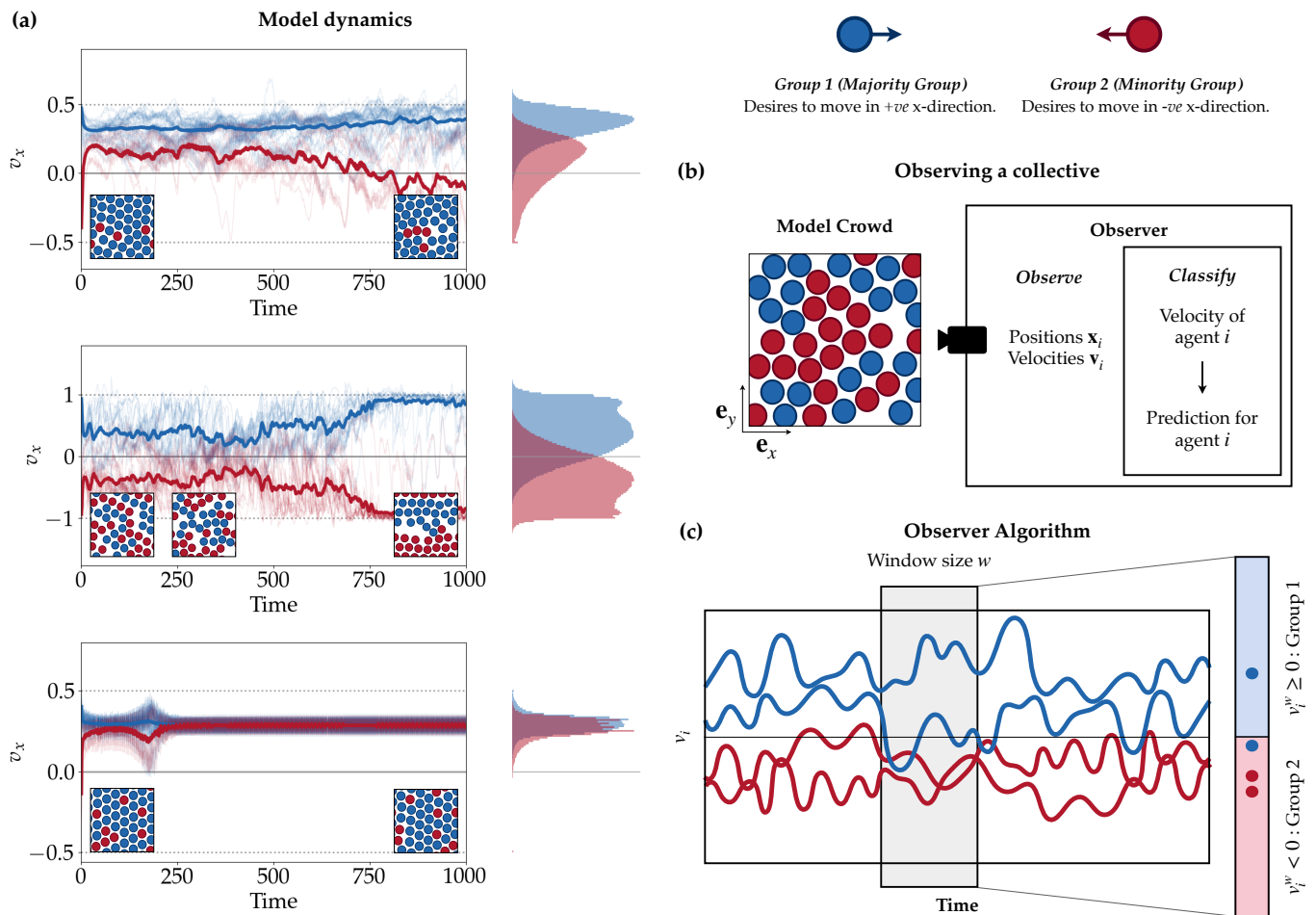


FIG. 1. Overview of the crowd dynamics and the simple observer algorithm where an agent is classified based on its velocity. (a) Examples of dynamics exhibited by the model at different parameter values. Plots show the horizontal velocities ($\mathbf{v}_{i,j} \cdot \mathbf{e}_x$) for the two groups of agents from a single run of the simulation. The faint blue and red traces are the individual agent velocities for Group 1 and Group 2 agents respectively. The thick blue and red traces are the average velocities (averaged over all agents in the group) for Group 1 and Group 2 agents. The dotted grey lines show $\pm s_0$, the desired x -velocities for the two groups. Insets show snapshots of the model dynamics at different time-points. The histograms show the distribution of agent velocities for the two groups, across all time-points, and across 100 simulations. Notice that the histograms have significant overlap, and histograms of the minority group (red in the top and bottom plots) are significantly shifted from their respective s_0 . (Also see Movie S1, appendix F) *Top*: Example of clustering ($N_r = 3/14, \rho = 0.46, s_0 = 0.5$). *Middle*: Example of lane formation ($N_r = 1/2, \rho = 0.46, s_0 = 1$). *Bottom*: Example of jamming ($N_r = 3/14, \rho = 0.58, s_0 = 0.5$). (b) The model crowd consists of two groups of agents, Group 1 (desired velocity towards the right, shown as blue) and Group 2 (desired velocity towards the left, shown as red). The observer observes the positions and velocities of agents in the crowd, and employs a classifier to classify agents as *Group 1/Group 2*. (c) Classification algorithm for the simple observer: For each agent, the classifier finds the average x -velocity of the agent within a short time window, and classifies the agent based on whether this velocity is positive or negative.

algorithm that classifies agents only based on its own movement information. Specifically, the observer uses the average velocity of the agent (over a window of length w) to classify the agent. An agent i is classified to be Group 1 if the average velocity v_i^w is positive, and Group 2 if v_i^w is negative. Figure 1(c) for a visual representation of the algorithm, and see appendix A for details.

For a given window, the number of misclassifications is identified by comparing the labels of the agents predicted by the observer to the ground-truth labels (the actual de-

sired directions for the agents, which are unknown to the observer). For each set of values for the parameters N_r and s_0 we compute the average number of misclassifications (n_m), averaged over multiple time windows and multiple independent realizations of the simulation.

This simple observer algorithm is the most straightforward way to classify agents. It assumes that the information necessary to classify an agent is fully contained in its own motion; and does not explicitly account for its interactions with the surroundings. The simple observer

will serve as a baseline to study the effect of emergent collective dynamics on classification, before we develop improved classification models.

Clustering facilitates movement and helps classification

In the context of stampede prevention, a typical N_r of interest would be $\mathcal{O}(\frac{1}{N})$, while in the context of pedestrian traffic in counter flows, it would be $\mathcal{O}(\frac{1}{2})$. Hence, to understand how the relative population sizes of the two groups in the composite crowd affect the group-dynamics—and consequently the ability of an observer to classify—we explore the entire range of N_r in our study and compute the average number of misclassifications n_m .

We identify three regimes in the range $N_r \in [\frac{1}{N}, \frac{1}{2}]$. When $N_r \ll \frac{1}{2}$, we find that the agents in the minority are well separated in space. We call this the *dilute regime*, where the agents in the smaller group do not form any clusters as they move and remain isolated from other agents of the same group. In this regime, at high enough crowd densities, the agents in the majority exert a force high enough to entrain (carry) those in the minority. The isolated agents in turn serve as obstacles to the flow of those in the majority resulting in fore-aft asymmetric local packing around the agent. When N_r is increased, agents in the minority start to form small clusters as time progresses. When N_r is close to or equal to $\frac{1}{2}$, we observe the formation of lanes, which increases the overall mobility (see Figure 1(a)).

We compute the number of misclassifications n_m as a function of N_r , as shown in Figure 2(a). We plot n_m corresponding to the larger and the smaller groups separately. The trends observed are qualitatively the same across different s_0 and ρ (Figure 5). In the dilute regime ($N_r \ll \frac{1}{2}$), the minority agents are isolated in a matrix of majority agents. Hence, nearly all of them will be pushed by the majority flow, and will end up being misclassified: as more minority agents are added, all of them will be misclassified, or in other words, n_m increases linearly with N_r . In the intermediate regime, n_m reaches a maximum point for the smaller group and then begins to decrease as $N_r \simeq \frac{1}{2}$. For the larger group, n_m shows a monotonic increase with N_r . It is interesting to observe the reduction of n_m with N_r close to the symmetric regime. When the number of agents in the minority group increase beyond a critical fraction, they begin to form clusters, as described earlier. Clusters begin to move through the crowd faster than when the agents were isolated—movement velocity of the cluster increases with cluster size. Once the movement commences, it reduces the probability of agents within the cluster to get misclassified.

The degree of clustering in the system can be quantified by computing the number of independent clusters c_{in} , for the agents in the minority group, as a function of N_r (Figure 2(b))—as the minority agents become more

and more clustered, c_{in} decreases. Note that *i*) agents were placed randomly in the crowd in our simulations, *ii*) if two agents of the same group are first Voronoi neighbors of each other, then they belong to the same cluster, *iii*) the periodic boundary has to be taken into account while identifying the number of clusters (c_{in}), and *iv*) an isolated agent is counted as its own cluster. We observe that c_{in} depends on N_r in a manner similar to n_m (compare panels (a) and (b) of Figure 2).

In the dilute regime, agents are isolated and each agent will belong to an independent cluster. As N_r increases, we observe the agents to form small local clusters which flattens the c_{in} curve. At even higher N_r , corresponding to the symmetric regime, system-spanning clusters are observed which result in the reduction of c_{in} . As the simulation proceeds, the number of clusters in the system would decrease due to passive cluster formation. However, we observe that the qualitative dependence on N_r is still preserved. Hence, it is clear that the trend in the number of misclassifications observed as a function of the number-ratio of agents in the minority group (n_m vs N_r) is simply due to the propensity of agents to form clusters in the crowd.

*Higher intrinsic speed may worsen classification:
a faster-is-slower effect*

Another important parameter to consider is s_0 , the intrinsic speed with which an agent propels in its desired direction. From an effort-viewpoint, one would expect the agents that try harder (large values of s_0) to move in their desired direction more easily. On the other hand, s_0 is also a measure of the difference in velocities (in the principle direction of motion) between the two groups of agents in the composite crowd. Hence, from a separation-viewpoint, one could expect higher rates of separation between agents belonging to different groups, for larger difference in property: for greater values of s_0 , agents can travel larger distances in a given amount of time.

We compute the number of misclassifications n_m as a function of s_0 for the asymmetric and symmetric cases, as shown in Figure 2(c). We observe that classification becomes easier as s_0 increases for the agents in the minority, as expected. The trend is similar across a range of N_r and ρ (Figure S2). However, for $N_r \neq \frac{1}{2}$, we find a non-monotonic dependence of n_m on s_0 for the agents in the majority. This suggests that even though the agents are trying harder to move in their desired directions, they are unable to. Upon further increase in s_0 , the decreasing trend begins to appear. Similar trends have been observed in other problems in the pedestrian dynamics and complex-flows communities and is commonly known as the *faster-is-slower* (FIS) effect. One of the first examples of this phenomenon is the case where a group of pedestrians exit a chamber through a narrow passage [27]. When agents try to exit faster, they tend to clog more often which results in intermittent flows

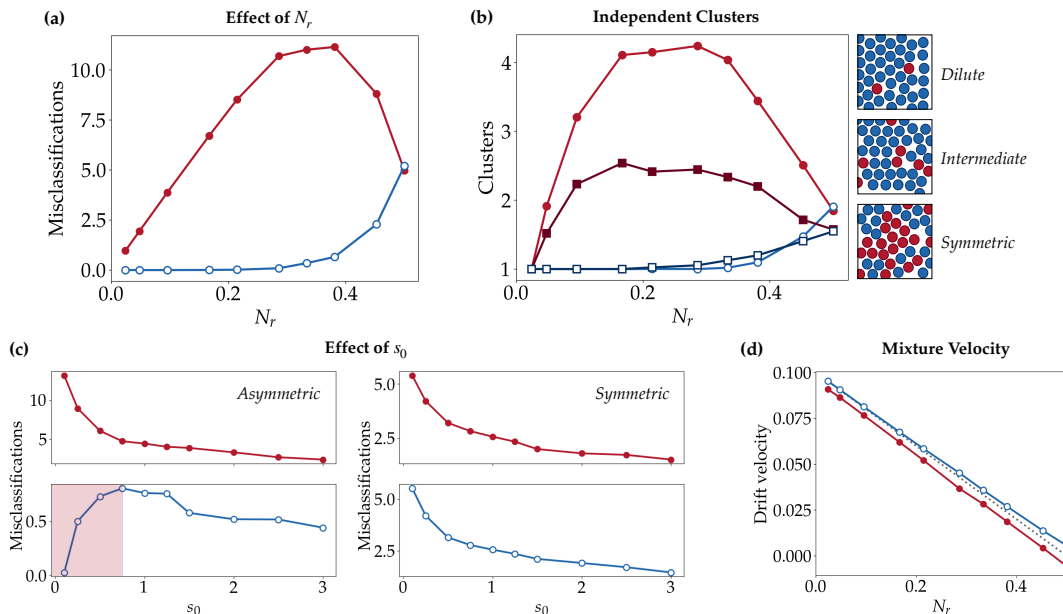


FIG. 2. Classification performance depends on the properties of the crowd, *viz.* composition of the composite crowd (N_r) and the intrinsic speed of the agents (s_0). For larger values of N_r , the agents start to form clusters and get classified more accurately. As the collective transitions from a frozen to a mobile state, agents in the majority group exhibit a faster-is-slower effect, where misclassifications with increasing s_0 . (a) Number ratio N_r has a non-monotonic effect on the number of misclassifications for the minority group, due to better clustering at higher N_r . Average number of misclassifications versus number-ratio N_r ($s_0 = 0.75$, $\rho = 0.58$). Misclassifications for the smaller group (red, filled circles) and larger group (blue, empty circles) are shown. (b) Number of independent clusters c_{in} versus N_r for the smaller (red, filled markers) and larger (blue, empty markers) groups. Initial (circle markers) and final (square markers) values are shown. Insets show snapshots of model systems at different values of N_r . Notice the fore-aft asymmetry around the minority (red) agents, neighbors are more tightly packed on the left than on the right. (c) The intrinsic speed s_0 affects misclassifications non-monotonically, highlighting a *faster-is-slower* effect for the majority group agents (see red highlighted region). Number of misclassifications versus s_0 for asymmetric (left, $N_r = 1/3$) and symmetric (right, $N_r = 1/2$) cases, for Group 1 (top, red) and Group 2 (bottom, blue) agents. $\rho = 0.46$. (d) Average drift speed of the frozen assembly versus N_r for the smaller group (red, filled circles) and larger group (blue, empty circles). The grey dotted line is the mixture velocity, given by $s_0(1 - 2N_r)$.

and increased exit-times [28]. While correlations can be drawn between the observed FIS effect with some flow-features in the crowd, the microscopic mechanisms leading to these features are not always clear [29].

To understand the microscopic origins of the FIS effect in our system, we investigate the motion of agents within the crowd. When s_0 is very small, the agents in the minority are trapped in a matrix of agents of the majority. This results in a frozen assembly that drifts in the desired direction of the majority, with a drift speed s_d . For a completely frozen assembly with no relative motion between agents, the expected velocity of the mixture of agents is simply the average of the individual $\mathbf{v}_{0,i}$ over the whole crowd, which equals $s_0(1 - 2N_r)$. The drift velocity s_d closely matches mixture velocity for small N_r (Figure 2(d)). When $N_r \simeq \frac{1}{2}$, the system size spanning clusters that are present lead to local re-arrangement of agents in the assembly that results in slight deviation in s_d at $N_r \simeq \frac{1}{2}$ in Figure 2(d).

Agents get trapped when the force that drives them in the direction they desire to move is smaller than the sum of all the forces due to the neighboring agents (in the x

direction), i.e., $\frac{m}{\tau}(\mathbf{v}_i \cdot \mathbf{e}_{-x} - s_0) < [\sum_{j \neq i} \mathbf{F}_{ij}(d_{ij}; \gamma)] \cdot \mathbf{e}_x$. When s_0 increases, agents in the minority (which were trapped so far) begin to break free and move through the crowd (Movie S2, appendix F). In other words, the crowd transitions from a *jammed state* to a *mobile state*. This disturbs the movement of the agents in the majority—which were more ‘fluid’ when the agents in the minority were trapped—giving rise to local jamming and subsequently, increased misclassification. This transition from the jammed state to the mobile state is the reason why n_m corresponding to the group in majority increases with s_0 —the observed FIS effect.

Correcting a misclassification

The simple observer algorithm classifies agents based on their net velocity measured over a time window w . For instance, when the observed velocity v_x^w of a Group 2 agent is positive, it will be classified as Group 1 incorrectly by the observer. Thus, correcting a misclassification would require the observer to classify the agent as

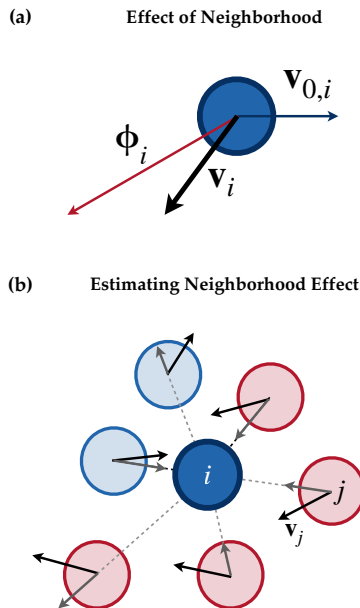


FIG. 3. Defining and quantifying the neighborhood parameter which depends on the states of the nearby neighboring agents. (a) The velocity \mathbf{v}_i of an agent can be decomposed into two components: $\mathbf{v}_{0,i}$, the intrinsic velocity of the agent, and $\boldsymbol{\phi}_i$, the influence of neighbors. As seen, $\mathbf{v}_{0,i}$ and \mathbf{v}_i may have different directions. (b) The neighborhood parameter $\hat{\boldsymbol{\phi}}_i$ is an estimate of $\boldsymbol{\phi}_i$, using velocities of neighbors. $\hat{\boldsymbol{\phi}}_i$ for an agent i (deep blue) is determined by the velocities of its neighbors (pale blue and red). The contribution of neighbor j is $\tilde{\mathbf{v}}_j$, the component of the velocity vector \mathbf{v}_j towards i . $\hat{\boldsymbol{\phi}}_i$ is a weighted sum of $\tilde{\mathbf{v}}_j$'s, weighted by a function of the distance between j and i .

belonging to Group 1 even if it exhibits a net movement in the negative direction. From the perspective of an observer, this is a counter-intuitive step: the observer has to differentiate agents in Group 2 from those in Group 1 that happen to move in the same x-direction. We need to ascertain the conditions under which an observer should swap the identified group-identity of the agent to correct a possible misclassification event.

An agent's neighborhood encodes information about its intrinsic direction

In the absence of interactions, an agent moves in its desired direction of motion with velocity s_0 , and classification is a trivial task. However, in the previous sections, we observed that inter-agent dynamics affect the dynamics in interesting ways, making agent classification a harder problem. An agent's movement is influenced by both its own intrinsic motion, as well as interaction-effects from its neighbors which can aid or hinder the motion. For improved classification performance, an observer needs to decouple the component of an agent's motion due to its intrinsic drive and the component of motion caused by these interaction effects.

In the current formulation of the classifier, the observer uses v_i as a proxy for the agent's desired velocity, $\mathbf{v}_{0,i}$. However, in reality, the observed \mathbf{v}_i is a combination of the agent's effort to move in $\mathbf{v}_{0,i}$ and the support or re-

sistance offered by the neighborhood $\boldsymbol{\phi}_i$.

$$v_i = \mathbf{v}_{0,i} \cdot \mathbf{e}_x + \boldsymbol{\phi}_i \cdot \mathbf{e}_x \quad (1)$$

See Figure 3(a) for an illustration. With this definition (Equation 1), the new classification criterion becomes,

$$\mathbf{v}_{0,i} \cdot \mathbf{e}_x = v_i - \phi_i > 0: \text{group 1} \quad (2)$$

$$\mathbf{v}_{0,i} \cdot \mathbf{e}_x = v_i - \phi_i < 0: \text{group 2} \quad (3)$$

where $\phi_i = \boldsymbol{\phi}_i \cdot \mathbf{e}_x$. In other words,

$$v_i > \phi_i: \text{group 1} \quad (4)$$

$$v_i < \phi_i: \text{group 2} \quad (5)$$

We now discuss an approach to estimate $\boldsymbol{\phi}_i$. As mentioned before, we use information from the local neighborhood to compute a *neighborhood parameter* $\hat{\boldsymbol{\phi}}_i$, which will serve as a surrogate for $\boldsymbol{\phi}_i$. To define $\hat{\boldsymbol{\phi}}_i$, we make the following observations and assumptions: *i*) an agent's motion is influenced predominantly by its immediate neighbors, *ii*) a neighbor can either aid or oppose the intrinsic movement of the agent, *iii*) the influence of a neighbor on an agent is dependent on the distance between them, and *iv*) the relative velocity of the neighbors, i.e. how fast the neighbor is approaching the position of the agent, can give an indication of the level of influence the neighbor has.

Based on this, we define $\hat{\phi}_i$ as a weighted sum of neighbor velocities, weighted by a function of the distance to the neighbor. The sum is scaled by a coefficient μ , which needs to be chosen appropriately to maximize classification performance. Appendix A provides details on the computation of $\hat{\phi}$; see Figure 3(b) for a simplified illustration. One could use a data-driven approach to estimate μ , by fitting a classifier model to labeled data. Since labeled data could be difficult to obtain in a general real world setting, a phenomenological approach to the problem becomes relevant. By enforcing that v_i and $\mu\varphi_i$ needs to be of the same scale, we estimate μ from the parameters of the model using a scaling analysis (see appendix A).

Recall that our classification criterion was $v_i \leq \phi_i$. In terms of the surrogate, this becomes $v_i \leq \hat{\phi}_i$, or $v_i \leq \mu\varphi_i$, where $\hat{\phi}_i = \mu\varphi_i$ and $\varphi_i = \mathbf{p}_i \cdot \mathbf{e}_x$. When $\mu = 0$, this reduces to the simple, agent-only observer algorithm. From a classification viewpoint, we have two features v_i and φ_i and the linear separator that divides the space into the binary classes (group 1 and 2), is $v_i = \mu\varphi_i$.

It is important to note that the neighborhood parameter is independent of the details of the simulation model. We use relative velocities of the neighbors as a proxy for inter-agent interactions; in other words, the neighborhood parameter only depends on the overall phenomenology of the crowd, and not on specific modeling assumptions.

Observing agents with the neighborhood-based observer

In what follows, we refer to the simple observer algorithm the *agent-only observer*, and the new algorithm as the *neighborhood observer*. In addition to computing the movement characteristics of just the agent v_i , the neighborhood observer calculates φ_i , which is a characteristic of its neighborhood. As before, we use the time-window-averaged versions of these quantities, denoted v_i^w and ϕ_i^w respectively. The parameter μ is calculated based on the knowledge of the global properties of the system— ρ and N_r .

Figure 4(a) illustrates how the neighborhood observer works. The plot shows the time-series of the (window-averaged) agent velocity v_i^w for a Group 1 agent. When it encounters Group 2 agents in its path, it may get pushed, causing v_i^w to dip below 0. The agent-only observer would then classify the agent—incorrectly—as Group 2: see blue shaded regions in the plot. However, the classification threshold for the neighborhood observer is ϕ_i^w (blue dashed line in the plot), incorporates information about the neighborhood of the agent, and can vary according to how much the agent is being pushed. Hence, the neighborhood observer is able to correctly classify the agent as Group 1 even when $v_i^w < 0$, i.e. the agent is moving in the negative x-direction. On the other hand, if the neighborhood observer over-estimates ϕ_i^w , we may misclassify agents even when the agent-only observer cor-

rectly classifies them. The bottom plot shows an example for a Group 1 agent moving in a well-laned configuration. Since all neighbors are moving with high velocity, the neighborhood observer occasionally over-estimates ϕ_i^w in the red shaded region and misclassifies the agent as Group 2; even though it is moving in the positive x-direction.

The stacked bar graphs in Figure 4(b) summarize the relative performances of the two observers. For asymmetric crowds ($N_r < 1/2$), the neighborhood observer performs better than the agent-only observer in terms of the total number of misclassifications: it does so by significantly improving the performance on the minority group, at the cost of a slight performance hit for the majority group. For symmetric crowds, the neighborhood observer performs slightly worse than the agent-only observer. To understand the reason behind this trend, we explore the mechanism of the neighborhood observer through a geometric lens.

Geometry of the neighborhood classifier

The neighborhood observer can alternatively be viewed as a linear classifier in the φ_i - v_i plane, with zero intercept and slope $1/\mu$ (see Equation A16). We now take a closer look at the geometry of the classification algorithm of the two observers. Consider the joint distribution of v_i^w versus φ_i^w . The agent-only observer does not take φ_i^w into consideration, hence its decision boundary corresponds to the vertical line through the origin. On the other hand, the decision boundary of the neighborhood observer is a line through the origin with slope $1/\mu$. The wedge-shaped regions in the first and third quadrants, marked A and B in Figure 4(c), are the regions where the predictions are different between the two observers. The relative performance of the neighborhood observer over the agent-only observer can be understood by taking a closer look at these regions.

Recall that in our simulations, the minority group is always Group 2, which desires to move in the negative x-direction. A Group 2 agent in Region A (and a Group 1 agent in Region B) will be incorrectly classified by the agent-only observer, but correctly classified by the neighborhood observer. On the other hand, a Group 1 agent in Region A (and a Group 2 agent in Region B) will be correctly classified by the agent-only observer but incorrectly classified by the neighborhood observer. In other words, the neighborhood observer improves the classification accuracy of Group 2 agents in Region A, at the cost of Group 1 agents. A similar statement can be made about Region B. The relative classification performances of the observers can now be understood in terms of the relative concentrations of agents in these regions.

We now discuss the effect of different model parameters on the classification performance of the neighborhood observer.

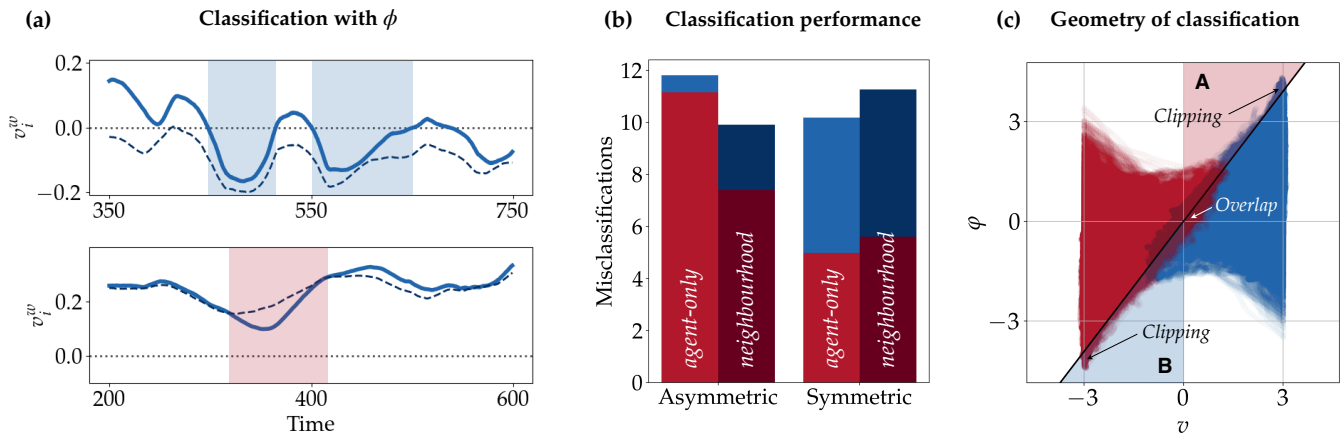


FIG. 4. The neighborhood observer classifies agents in the minority-group more accurately at the expense of those in the majority-group, improving the overall performance for asymmetric crowds. (a) Visualizing the working of the neighborhood classifier: The top panel shows an example where the neighborhood observer works well. The blue solid line is the observed velocity v_i^w of a Group 1 agent, and the blue dashed line is the neighborhood parameter ϕ_i^w . The blue shaded regions are the time-points when the agent-only observer misclassifies the agent as Group 2, but the neighborhood observer correctly identifies as Group 1. The bottom panel shows an example where the neighborhood observer makes an error. In the red shaded region, the neighborhood observer classifies the agent incorrectly as Group 2, despite the agent moving in the positive x -direction. (b) Comparison of classification performances of the two observers. In the asymmetric case ($N_r = 16/21$), the neighborhood observer makes fewer errors for the minority group (Group 2, red bars), but makes slightly more errors for the majority group (Group 1, blue bars). The total number of errors is lower for the neighborhood observer. In the symmetric case, the neighborhood observer performs worse than the agent-only observer. ($s_0 = 0.75, \rho = 0.58$) (c) A schematic showing the geometry of classification. the agent-only observer and the neighborhood observer will have different predictions for agents in the shaded wedge-shaped region (marked A, B). Group 1 agents (blue) in A and Group 2 agents (red) in B will be correctly flipped by the neighborhood observer. On the other hand, Group 1 agents in B and Group 2 agents in A will be incorrectly flipped. The relative classification performances of the observers is determined by the number of correct versus incorrect flips.

Neighborhood observer improves classification for asymmetric crowds

For asymmetric crowds ($N_r < \frac{1}{2}$), the neighborhood observer outperforms the agent-only observer by making a considerable improvement in classifying the minority group agents while performing slightly worse on the majority group (Figure 4(b)). In the asymmetric regime, agents from the minority group (Group 2) are more prone to get pushed by agents from the majority group (Group 1), causing the agent-only observer to misclassify them. However, the neighborhood of any agent will consist mostly of majority agents, causing ϕ_i^w to be large. Hence, the neighborhood observer is able to correctly identify many of these agents. That is, even though these agents are being pushed in the positive x -direction, the neighborhood observer correctly classifies them as Group 2. However, this comes at a slight cost of classification performance for the majority group—since ϕ_i^w is usually large, a slow-moving majority agent can have $v_i^w < \phi_i^w$ and can get misclassified.

For symmetric crowds, no one group gets an advantage over the other in getting classified correctly.

Dense and slow crowds are harder to classify for both observers

When density ρ is small, the agents are sparsely distributed and have relatively more space to move around. This means a clear separation of the $v_i - \phi_i$ distributions of Group 1 and Group 2 agents (Figure 8), resulting in almost no misclassifications for either observer. As density increases, there is less space for free movement and the agents are blocked more often: this causes a greater overlap in the distributions, making classification harder for both observers.

The intrinsic velocity s_0 has an effect complementary to ρ in the classification performance. When s_0 is low, the agents move almost like a frozen assembly, resulting in a high number of misclassifications for the agent-only observer. However, since ϕ is also correspondingly low, there is a large overlap in the distributions of the two groups. Hence, the neighborhood observer cannot improve performance very much.

(See Figure 5, 6 for a quantitative comparison between the performances of the two observers as a function of the parameters N_r, ρ and s_0 .)

Modes of error for the neighborhood observer

Figure 4(c) shows the key features of the neighborhood classifier in terms of the distributions of v_i^w and φ_i^w . In the ideal case, the classification boundary should split the Group 1 and Group 2 agents (blue and red points in the figure respectively). However, this is not always the case, and errors can occur due to two main reasons.

Firstly, the classification boundary may ‘clip’ the distributions of Group 1 and Group 2 near high-velocity regions. For example, for symmetric or near-symmetric crowds, the neighborhood observer is found to clip a small portion of the regions corresponding to large $|v_i^w|$ (see Figure 4). This usually happens when the agent is moving in a well-laned configuration (Movie S3, appendix F). As an assembly of agents interact to form lanes, they form heterogeneous regions with high and low densities. When agents are densely packed locally, they have a larger φ_i than that predicted by the scaling which uses the length scale $\frac{1}{\sqrt{\rho}}$, resulting in inaccurate classifications. Note that the clipping effect is due to mis-estimation of the parameter μ ; an alternate classifier with a slightly rotated decision boundary can get rid of the problem. An alternate approach would be a non-linear classifier that takes into account the fact that agents with high horizontal velocities are highly likely to be moving on their own volition (and not pushed).

Secondly, in any region in the distribution where Group 1 and Group 2 overlap, the observer is bound to make some misclassifications. The size of this region depends on parameters s_0 and ρ , and contains instances of slow-moving agents: usually caught in a blockade. This is a fundamental limitation that may be difficult to overcome: in these overlap regions, there is no discernible difference between the groups in the velocities or neighborhood characteristics between the two groups. Even an optimal classifier trained from data (Figure 9) is unable to significantly improve classification performance in this scenario.

DISCUSSION

In this article, we set out to understand how the classification process of an observer is connected to the microscopic details of the crowd dynamics. We begin with a simple observation/classification technique based on the measured velocity of agents (averaged over a small time window). We show how the relative population size of the groups can affect the way clusters are formed as agents move, which affect the propensity to get classified accurately. We find that a crowd can exhibit counter-intuitive dynamics, where agents get misclassified a lot more when they try harder to move past each other—similar to the so-called faster-is-slower (FIS) effect. As the intrinsic velocity increases, we find a transition between a frozen state—where minority agents are embedded in a matrix of the majority agents—to a mobile state—where the

there is relative motion between agents. This transition to the mobile state causes obstructions to the movement of the majority agents, giving rise to the FIS effect mentioned above.

Going further, we developed an observer that classifies an agent based on information not just about itself, but also about its neighbors. Although simple in principle, this neighborhood observer does something quite non-trivial: it distinguishes between a Group 1 and a Group 2 agent even when they are moving in the same direction with identical velocities. The fact that the neighborhood observer takes into account the influence of the neighboring agents for classification helps it to ‘read the mind’ of the focal agent by distinguishing when it is moving on its own volition versus when it is being pushed.

Note that both the observers treat the time windows as independent: when making predictions for a given time window, the observers do not use information from previously observed windows. One could conceive an observer that uses historical information and updates beliefs with time, perhaps in a Bayesian fashion. We do not explore this approach; our goal is to explore techniques that work with minimal observations, and to understand how instantaneous and short-term dynamics in the system affects our ability to classify agents.

The 2D classifier that the neighborhood observer employs is not data-driven: the decision boundary is not obtained by a data fit, but is instead derived from scale considerations. This makes our approach applicable in scenarios where labeled data is not easy to obtain. This also makes our classifier readily interpretable, as it is well-grounded in the physics of the problem. The assumptions the classification algorithm makes about the details of the model are minimal. Specifically, the neighborhood parameter is computed based on neighbor velocities only, and is independent of specific modeling assumptions. It is not based on the specific nature and functional form of inter-agent interactions.

We now discuss some ways to improve the classification performance of the neighborhood observer. Firstly, if labeled data (i.e. data where the group memberships of agents are known) is readily available, we can fit a linear classifier to the data to get improved results (Figure 9). When a classifier is fit in this manner, it will not be susceptible to unfulfilled assumptions in computing μ , such as mismatch between local and global densities. Secondly, notice that an agent moving in its desired direction will move faster than when it is pushed in the opposite direction. If we can estimate the maximum velocity with which an agent can move when being pushed, this can be incorporated into a classification logic. The classifier will now be a hybrid algorithm, with hard velocity thresholds for which it will be classified into Group 1 or Group 2, and a region in between where a linear classifier akin to the neighborhood observer operates. This will get rid of the problem of clipping we observed above. The hard thresholds could be derived from data, making this a hybrid classifier.

An orthogonal approach is to build a purely data-driven classifier based on neural networks. One could build a neural-net classifier that takes as input the positions and velocities of the focal agent and its neighbors, and makes predictions. Given enough labelled data, such classifiers can learn high-quality, low-dimensional feature representations that can make effective predictions. To be effective, such neural network classifiers should be informed and constrained by the physics and inherent symmetries of the problem. In our case, it means that the neural network should respect the rotational and translational invariances of the system, and should be invariant to any permutation of the agent ordering. Constraints such as these should be built in to the neural network design. There is an emerging body of research in graph neural networks [30, 31] and physics-informed deep learning [32, 33] which can be explored in this regard. Building neural network classifiers for collective dynamics and studying their feature representations is an exciting research direction.

Classifying agents in a real crowd is a much harder problem to study in comparison to the model system we investigate in this article. We assume the composite crowd to be *bi-disperse*—consisting of two groups of agents and *uniform*—indistinguishable from each other. However, agents in a real crowd are seldom uniform and one does not really know the total number of *distinct groups* they fall under. Note here that in our study, we assumed that the observer knows the crowd to be bi-disperse. In fact, when the observer attempts to infer the *rule* that the agents follow, it never uncovers the same value for $v_{0,i}$. Almost always, the observer infers a different value for each agent in a certain group. Simply put, even a uniform group of agents are identified as

non-uniform due to the differences in the conditions they experience as they move in the crowd. Hence, it will be even harder to identify agents in poly-disperse settings (real crowds) where the number of groups are not known a priori.

Therefore, it is worth reiterating that the goal of this study is to understand the ways in which the microscopic properties of a crowd affect the classification performance of an observer that is only privy to observables such as agent positions and velocities. We study this in the context of a model system, which is an idealised version of collective systems in the real world. For this reason, hunting for the best data-driven classifier to solve this specific problem may not be very useful; such a classifier will not be transferable to a real-world crowd as real-world crowds can be polydisperse and can involve many complex interactions not included in our model. Hence, our main goal was to understand how the microscopic properties and inter-agent interactions can affect classification. A clear understanding of this relationship is essential to solve similar problems in real-world crowds. Our phenomenological approach to the classification problem is a first step towards hybrid techniques, where a data-driven approach is combined with domain-specific understanding of the crowd dynamics to build better observer models.

ACKNOWLEDGMENTS

The authors would like to thank DST INSPIRE faculty award for the funding. The authors thank Jason Ryan Picardo, Ganapathy Ayappa, Vishwesh Guttal, Vivek Jadhav, Basil Thurakkal and Harishankar Muppurala for critical readings of the manuscript.

-
- [1] R. Candelier and O. Dauchot, Journey of an intruder through the fluidization and jamming transitions of a dense granular media, *Physical Review E - Statistical, Nonlinear, and Soft Matter Physics* **81**, 1 (2010), arXiv:0909.4628.
 - [2] T. Thorsen, R. W. Roberts, F. H. Arnold, and S. R. Quake, Dynamic Pattern Formation in a Vesicle-Generating Microfluidic Device, *Physical Review Letters* **86**, 4163 (2001).
 - [3] S. Kamijo, Y. Matsushita, K. Ikeuchi, and M. Sakauchi, Traffic monitoring and accident detection at intersections, *IEEE Conference on Intelligent Transportation Systems, Proceedings, ITSC* **1**, 703 (1999).
 - [4] V. Murino, M. Cristani, S. Shah, and S. Savarese, The Group and Crowd Analysis Interdisciplinary Challenge, in *Group and Crowd Behavior for Computer Vision* (Elsevier, 2017) pp. 1–11.
 - [5] J. Jhavar, R. G. Morris, U. Amith-Kumar, M. D. Raj, T. Rogers, H. Rajendran, and V. Guttal, Noise-induced schooling of fish, *Nature Physics* **16**, 488 (2020).
 - [6] A. Cavagna and I. Giardina, The seventh starling, *Significance* **5**, 62 (2008).
 - [7] J. E. Herbert-Read, A. Perna, R. P. Mann, T. M. Schaerf, D. J. T. Sumpter, and A. J. W. Ward, Inferring the rules of interaction of shoaling fish, *Proceedings of the National Academy of Sciences* **108**, 18726 (2011), <https://www.pnas.org/content/108/46/18726.full.pdf>.
 - [8] K. Klemm, M. Á. Serrano, V. M. Eguíluz, and M. San Miguel, A measure of individual role in collective dynamics, *Scientific reports* **2**, 1 (2012).
 - [9] R. Lukeman, Y.-X. Li, and L. Edelstein-Keshet, Inferring individual rules from collective behavior, *Proceedings of the National Academy of Sciences* **107**, 12576 (2010), <https://www.pnas.org/content/107/28/12576.full.pdf>.
 - [10] Y. Katz, K. Tunstrøm, C. C. Ioannou, C. Huepe, and I. D. Couzin, Inferring the structure and dynamics of interactions in schooling fish, *Proceedings of the National Academy of Sciences* **108**, 18720 (2011), <https://www.pnas.org/content/108/46/18720.full.pdf>.
 - [11] F. J. H. Heras, F. Romero-Ferrero, R. C. Hinz, and G. G. de Polavieja, Deep attention networks reveal the rules of collective motion in zebrafish, *PLOS Computational Biology* **15**, 1 (2019).
 - [12] M. Muramatsu, T. Irie, and T. Nagatani, Jamming tran-

- sition in pedestrian counter flow, *Physica A: Statistical Mechanics and its Applications* **267**, 487 (1999).
- [13] J. Dzubiella, G. P. Hoffmann, and H. Löwen, Lane formation in colloidal mixtures driven by an external field, *Physical Review E - Statistical Physics, Plasmas, Fluids, and Related Interdisciplinary Topics* **65**, 1 (2002).
- [14] J. Chakrabarti, J. Dzubiella, and H. Löwen, Dynamical instability in driven colloids, *Europhysics Letters* **61**, 415 (2003).
- [15] J. Delhommelle, Should "lane formation" occur systematically in driven liquids and colloids?, *Physical Review E - Statistical, Nonlinear, and Soft Matter Physics* **71**, 1 (2005).
- [16] Y. Tao and L. Dong, A Cellular Automaton model for pedestrian counterflow with swapping, *Physica A: Statistical Mechanics and its Applications* **475**, 155 (2017).
- [17] N. Bain and D. Bartolo, Critical mingling and universal correlations in model binary active liquids, *Nature Communications* **8**, 1 (2017), arXiv:1612.02565.
- [18] A. Poncet, O. Bénichou, V. Démery, and G. Oshanin, Universal Long Ranged Correlations in Driven Binary Mixtures, *Physical Review Letters* **118**, 118002 (2017), arXiv:1608.00094.
- [19] C. Reichhardt and C. J. Reichhardt, Velocity force curves, laning, and jamming for oppositely driven disk systems, *Soft Matter* **14**, 490 (2018), arXiv:arXiv:1707.09438v1.
- [20] L. Liu, K. Li, X. L. Zhou, L. L. He, and L. X. Zhang, Controllable laning phase for oppositely driven disk systems, *Chinese Physics B* **28**, 10.1088/1674-1056/ab4e86 (2019).
- [21] D. Helbing, L. Buzna, A. Johansson, and T. Werner, Self-Organized Pedestrian Crowd Dynamics: Experiments, Simulations, and Design Solutions, *Transportation Science* **39**, 1 (2005).
- [22] C. Feliciani and K. Nishinari, Empirical analysis of the lane formation process in bidirectional pedestrian flow, *Physical Review E* **94**, 10.1103/PhysRevE.94.032304 (2016).
- [23] K. R. Sütterlin, A. Wysocki, A. V. Ivlev, C. R ath, H. M. Thomas, M. Rubin-Zuzic, W. J. Goedheer, V. E. Fortov, A. M. Lipaev, V. I. Molotkov, O. F. Petrov, G. E. Morfill, and H. Löwen, Dynamics of lane formation in driven binary complex plasmas, *Physical Review Letters* **102**, 1 (2009), arXiv:0812.3091.
- [24] T. Vissers, A. Wysocki, M. Rex, H. Löwen, C. P. Royall, A. Imhof, and A. Van Blaaderen, Lane formation in driven mixtures of oppositely charged colloids, *Soft Matter* **7**, 2352 (2011).
- [25] D. Helbing, I. J. Farkas, and T. Vicsek, Freezing by Heating in a Driven Mesoscopic System, *Physical Review Letters* **84**, 1240 (2000).
- [26] T. Hastie, R. Tibshirani, and J. Friedman, Overview of supervised learning, in *The elements of statistical learning* (Springer, 2009) pp. 9–41.
- [27] D. Helbing, I. Farkas, and T. Vicsek, Simulating dynamical features of escape panic, *Nature* **407**, 487 (2000), arXiv:0009448 [cond-mat].
- [28] A. Garcimartín, I. Zuriguel, J. M. Pastor, C. Martín-Gómez, and D. R. Parisi, Experimental evidence of the "faster is slower" effect, *Transportation Research Procedia* **2**, 760 (2014).
- [29] C. Gershenson and D. Helbing, When slower is faster, *Complexity* **21**, 9 (2015), arXiv:1506.06796.
- [30] J. Zhou, G. Cui, S. Hu, Z. Zhang, C. Yang, Z. Liu, L. Wang, C. Li, and M. Sun, Graph neural networks: A review of methods and applications, *AI Open* **1**, 57 (2020).
- [31] M. M. Bronstein, J. Bruna, T. Cohen, and P. Veličković, Geometric deep learning: Grids, groups, graphs, geodesics, and gauges (2021).
- [32] G. E. Karniadakis, I. G. Kevrekidis, L. Lu, P. Perdikaris, S. Wang, and L. Yang, Physics-informed machine learning (2021).
- [33] M. Raissi, P. Perdikaris, and G. E. Karniadakis, Physics-informed neural networks: A deep learning framework for solving forward and inverse problems involving nonlinear partial differential equations, *Journal of Computational Physics* **378**, 686 (2019).
- [34] W. B. Krantz, *Scaling analysis in modeling transport and reaction processes: a systematic approach to model building and the art of approximation* (2007) p. 547.

Appendix A: Methods

Crowd model

Agents are modelled as apolar discs in a 2D-periodic domain. Their dynamics is governed by the following equations:

$$m \frac{d\mathbf{v}_i}{dt} = \frac{m}{\tau} (\mathbf{v}_{0,i} - \mathbf{v}_i) + \sum_{j \neq i} \mathbf{F}_{ij} \quad (\text{A1})$$

$$\mathbf{v}_{0,i} = \begin{cases} +s_0 \mathbf{e}_x & i \in \text{Group 1} \\ -s_0 \mathbf{e}_x & i \in \text{Group 2} \end{cases} \quad (\text{A2})$$

$$\mathbf{F}_{ij} = \begin{cases} -\gamma (d_{ij} - 2R)^{-3} \hat{\mathbf{d}}_{ij} & d_{ij} < l_{cr} \\ 0 & \text{otherwise} \end{cases} \quad (\text{A3})$$

The intrinsic velocity $\mathbf{v}_{0,i}$ has a magnitude s_0 , and is directed along the positive or negative x-direction depending on the group of the individual (see Equation A2). The inter-individual force \mathbf{F}_{ij} is a repulsive force, and decays as a power-law with distance. To prevent collisions, \mathbf{F}_{ij} is chosen such that its magnitude blows up to infinity when the agent boundaries touch ($d_{ij} = 2R$). To avoid spurious interactions between far-off agents, \mathbf{F}_{ij} is set to 0 beyond a cut-off radius (see Equation A3). m is the mass of an individual agent, τ is the inertial time-scale of the system, and γ determines the strength of the inter-agent interactions. \mathbf{e}_x denotes the unit vector along x-direction. We define the packing density ρ as the number of agents per unit area.

Simulations

Agents are placed randomly on a 2-D periodic domain, ensuring that there are no overlaps. Group identities of the agents are assigned randomly: for a given value of the number ratio (N_r), $N_r \cdot N$ randomly chosen agents are

assigned to Group 2 and the remaining agents to Group 1. We focus on the effect of three parameters, N_r , ρ and s_0 , we vary these over the following ranges: $\rho \in [0.22, 0.58]$, $N_r \in [\frac{1}{N}, \frac{1}{2}]$, $s_0 \in [0.1, 3]$. Due to the inherent symmetry between the groups, we can ignore $N_r > \frac{1}{2}$ without loss of generality. As a result, Group 1 is always the majority group in our simulations.

The following parameters were fixed: $m = 1, \tau = 0.2, \gamma = 0.2, R = 1, l_{cr} = 3$.

The parameters N_r , ρ and s_0 were varied over the following sets.

$$\begin{aligned} N_r &\in \{1/42, 1/21, 2/21, 1/6, 3/14, 2/7, 1/3, 8/21, 19/42, 1/2\} \\ s_0 &\in \{3, 2, 1.5, 1, 0.75, 0.5, 0.25, 0.1\} \\ \rho &\in \{0.57706, 0.45792, 0.3722, 0.30847, 0.25981, 0.22182\} \end{aligned}$$

The total number of agents in the simulations was 42. Since $N_r < 1/2$, Group 2 was always the minority group.

Phenomena such as laning, clustering, etc. will depend upon the initial conditions of the simulations. Hence, we perform 100 simulations for each set of parameter values.

Simple observer model (agent-only observer)

A simple but effective approach for classification is to classify agents based on their observed direction of motion. For a better estimate that eliminates transient fluctuations, one may use the average velocity computed over a time-window. Therefore, our simple observer algorithm proceeds as follows. First, the observer computes the average velocity v_i^w of the agents, averaged over a time-window of length w .

$$v_i^w = \langle \mathbf{v}_i \cdot \mathbf{e}_x \rangle_w \quad (\text{A4})$$

The observer classifies an agent based on the net direction of motion during this window, i.e. the sign of v_i^w :

$$v_i^w \geq 0 : \text{Group 1} \quad (\text{A5})$$

$$v_i^w < 0 : \text{Group 2} \quad (\text{A6})$$

In a real-world scenario, an observer has to tackle the problem of sensor noise that corrupts the data. However, we make the simplifying assumption that the observer can observe the system perfectly without noise; the only unknown is the individual group identities of the agents, which the observer desires to infer.

In our analyses, we used a window-length $w = 50$. A shorter window corresponds to decision-making with fewer data points, while a larger window size may result in improved classification performance. The exact window length does not qualitatively affect the results, we verified this by repeating our analysis with several window sizes between 25 and 100.

Neighborhood observer model

We define a neighborhood parameter $\hat{\boldsymbol{\phi}}_i$ evaluated for each individual i , using information from its first Voronoi neighbors \mathcal{N} as follows:

$$\hat{\boldsymbol{\phi}}_i = \mu \sum_{\forall j \in \mathcal{N}} f(r_{ij}) [\mathbf{v}_j \cdot \mathbf{e}_{ji}] \mathbf{e}_{ji} \quad (\text{A7})$$

The parameter $\hat{\boldsymbol{\phi}}_i$ is a vector that contains the net effect of all the neighbors (in \mathcal{N}) on the agent i . Agents interact as they approach each other, hence the velocities are resolved along the direction vectors of the line joining the two agents' center of masses \mathbf{e}_{ji} . In addition, a weighting $f(r_{ij})$, is used to capture the effect of distance from the focal agent i : agents far away will have lesser impact on the motion of agent i . The choice of f is somewhat arbitrary, as long as it is a monotonically decreasing function that does not decrease 'too fast'. For the purpose of this article, we use a Gaussian kernel of the form $e^{(-r_{ij}/\epsilon)^2}$ as the weighting function, where $\epsilon = 3R$ is the length scale corresponding to the decay of f (see Appendix C and Figure 7) for an extended discussion on the choice of f). The choice of f and the neighborhood being chosen (Voronoi in our case) decide the local neighborhood being considered for an agent, the exact choices for these are not very crucial.

μ is a scaling parameter which needs to be fixed appropriately. We can employ a data-based approach to estimate the optimal μ that maximizes accuracy of classification using data from our simulations along with the knowledge of their actual group-identities as labels. As the availability of labeled data is not a given in real-crowd problems, we turn towards exploring the phenomenology (Equation 1) to derive a scaling for the parameter μ .

We can begin by employing an order-one scaling analysis[34] on Equation 1. We express each of the variables x as a product of an $o(1)$ variable denoted as \bar{x} and an order of magnitude x_s .

$$v_s \bar{v}_i^m = v_s \bar{\mathbf{v}}_{0,i} \cdot \mathbf{e}_x + \mu \varphi_s \bar{\varphi}_i \quad (\text{A8})$$

$$\bar{v}_i^m = \bar{\mathbf{v}}_{0,i} \cdot \mathbf{e}_x + \frac{\mu \varphi_s}{v_s} \bar{\varphi}_i \quad (\text{A9})$$

We choose a scale $\varphi_s = \frac{v_s}{\mu}$, to make sure that Equation A9 is balanced and all the terms contribute to \bar{v}_i^m , as assumed initially when proposing Equation 1. Say, for instance, if $\varphi_s \ll \frac{v_s}{\mu}$, then Equation A9 becomes similar to Equation A4, as in our original formulation.

We can now resort to scaling Equation A7 and use the

relation $\varphi_s = \frac{v_s}{\mu}$ which gives rise to,

$$\frac{v_s}{\mu} \bar{\varphi}_i = f_s \sigma_s v_s \sum_{\forall j \in \mathcal{N}} \bar{f}(r_{ij}) [\bar{\mathbf{v}}_j \cdot \mathbf{e}_{ji}] \mathbf{e}_{ji} \cdot \mathbf{e}_x \quad (\text{A10})$$

$$\bar{\varphi}_i = \mu f_s \sigma_s \sum_{\forall j \in \mathcal{N}} \bar{f}(r_{ij}) [\bar{\mathbf{v}}_j \cdot \mathbf{e}_{ji}] \mathbf{e}_{ji} \cdot \mathbf{e}_x \quad (\text{A11})$$

$$\mu = \frac{1}{f_s \sigma_s} \quad (\text{A12})$$

A scaling for μ as shown in Equation A12, arises naturally from Equation A11, when we try to balance the terms. A suitable scale for f would be,

$$f_s = e^{-\frac{1}{\rho \epsilon^2}} \quad (\text{A13})$$

where $\sqrt{\frac{1}{\rho}}$ is the typical length scale corresponding to a crowd with a global packing density ρ . σ_s is the scale of velocity that arises as a result of the composite nature of the crowd. If all the agents in the neighborhood \mathcal{N} belong to the same group, then σ_s simply takes a value of the mean number of neighbors (which we can assume as 6, as the agents in our system are spherical and interact isotropically). On the other hand, if only half the agents in \mathcal{N} belong to one group, the effect cancels out. Hence, σ_s is the expected value of the excess agents in the majority group in \mathcal{N} .

If we assume that the probability of finding an agent from a certain group is independent of other agents in the vicinity, then one can write the expression for the probability ($p_k^{N_r}$) of finding k individuals of group 2 in \mathcal{N} as in Equation A14.

$$p_k^{N_r} = \binom{l}{k} N_r^k (1 - N_r)^{6-k} \quad (\text{A14})$$

where $|\mathcal{N}| = l$. We take $l = 6$ for computations. When there are k agents of group 2, the contribution to σ_s is $|6 - 2k|$. Using Equation A14, we can evaluate the expected value σ_s as follows.

$$\sigma_s = \sum_{k=0}^6 p_k^{N_r} |6 - 2k| \quad (\text{A15})$$

Combining all the terms in Equation A12, using Equation A13 and A15, we get the final equation of the linear classifier as shown in Equation A16.

$$v_i^m - \left(\frac{e^{\frac{1}{\rho \epsilon^2}}}{\sum_{k=0}^6 p_k^{N_r} |6 - 2k|} \right) \varphi_i = 0 \quad (\text{A16})$$

Where the parameter μ is,

$$\mu = \left(\frac{e^{\frac{1}{\rho \epsilon^2}}}{\sum_{k=0}^6 p_k^{N_r} |6 - 2k|} \right) \quad (\text{A17})$$

Statistical significance

The average number of misclassifications n_m was computed as an average over 100 simulations and 951 window positions (all positions of a window of length 50 over a time-series of length 1000). Therefore, the confidence intervals for n_m are too small to be visible in the plots, and are ignored in Figures 2 and 4. We used a Wilcoxon signed-rank test to test if n_m is significantly different between the agent-only observer and the neighborhood observer. Due to the very large number of samples, p-values for all tests were 0 up to machine precision.

Appendix B: Model parameters and classification performance

Figures 5 and 6 show the variation of classification performance over a wide range of parameters. The number of misclassifications by both observers is shown.

Figure 2(a) of main text shows the effect of N_r on the number of misclassifications for a particular ρ and s_0 ($s_0 = 0.75$, $\rho = 0.58$). As s_0 and ρ are varied, the plots get scaled accordingly, but the essential qualitative features of the plots are not affected (Figure 5). The case is similar for misclassifications versus s_0 plots (Figure 6).

Also, the qualitative features of the misclassification curves for the neighbourhood observer are similar to that of the agent-only observer.

Appendix C: Choice of weighting function f

The choice of the weighting function f in Section IV-A merits some discussion. Clearly, we need the weighting function to assign high weights to nearby neighbours and low weights to ones that are farther away, i.e. we need an f such that $f(r)$ decreases monotonically with r , where r is the distance from the focal agent.

Besides, our computation of the scaling factor is dependent on f :

$$\mu = \frac{1}{\sigma_s f_s} = \frac{1}{\sigma_s f(L_s)} \quad (\text{C1})$$

where L_s is a length-scale, which we choose to be $\sqrt{\frac{1}{\rho}}$. However, this is an estimate based on the global density parameter: as discussed in Section IV-C, phenomena like lane formation can cause agents to have very different local densities in their neighbourhood, causing the effective length scale to be different from $\sqrt{\frac{1}{\rho}}$. Therefore, to prevent large errors in the estimation of μ in these cases, we need to ensure that f is robust to mis-estimation of L_s , i.e. does not vary too fast in the vicinity of L_s . We chose $f(r) = e^{-r^2/\epsilon}$ with $\epsilon = 3$ for our analysis.

Figure 7 shows a comparison between two choices of f : $f_{\text{cubic}}(r) = \frac{1}{r^3}$ and $f_{\text{exp}}(r) = e^{-r^2/\epsilon}$. Over a range

of typical densities, there is a larger relative variation in $f_{\text{poly}}(L_s)$, which translates to a very large variation in μ . Therefore, small mismatches between the local density around an agent and the global density can result in a large mis-estimation of μ .

Appendix D: Effect of parameters on distributions

Figure 8 shows how the model parameters affect the $v_i - \phi_i$ distributions. See figure caption for details, and the main text for a discussion from the viewpoint of dynamics.

Appendix E: Learning μ from data

In the paper, we discussed an approach to compute μ from the global parameters of the system, ρ and N_r , using phenomenological considerations. When labelled

training data (i.e. crowd data where individuals are already marked as Group 1 or Group 2) is readily available, an alternate approach would be to fit a linear classification model to the data.

We explore this by fitting a linear SVM (support vector machine) with 0 intercept to the data. Assuming the training-algorithm converges well, this will give us the *optimal* linear classifier; optimal in the sense that it will be the best line that classifies agents on the $v_i^w - \phi_i^w$ plane. This classifier overcomes the problem of ‘clipping’ we observed, and outperforms the agent-only observer for all parameter values. Figure 9 shows how the decision boundary of the SVM avoids the clipping problem, and compares the performance of the three algorithms.

Appendix F: Supplementary videos

For supplementary videos, see: <https://www.dannyraj.com/obsinf-supp-info>

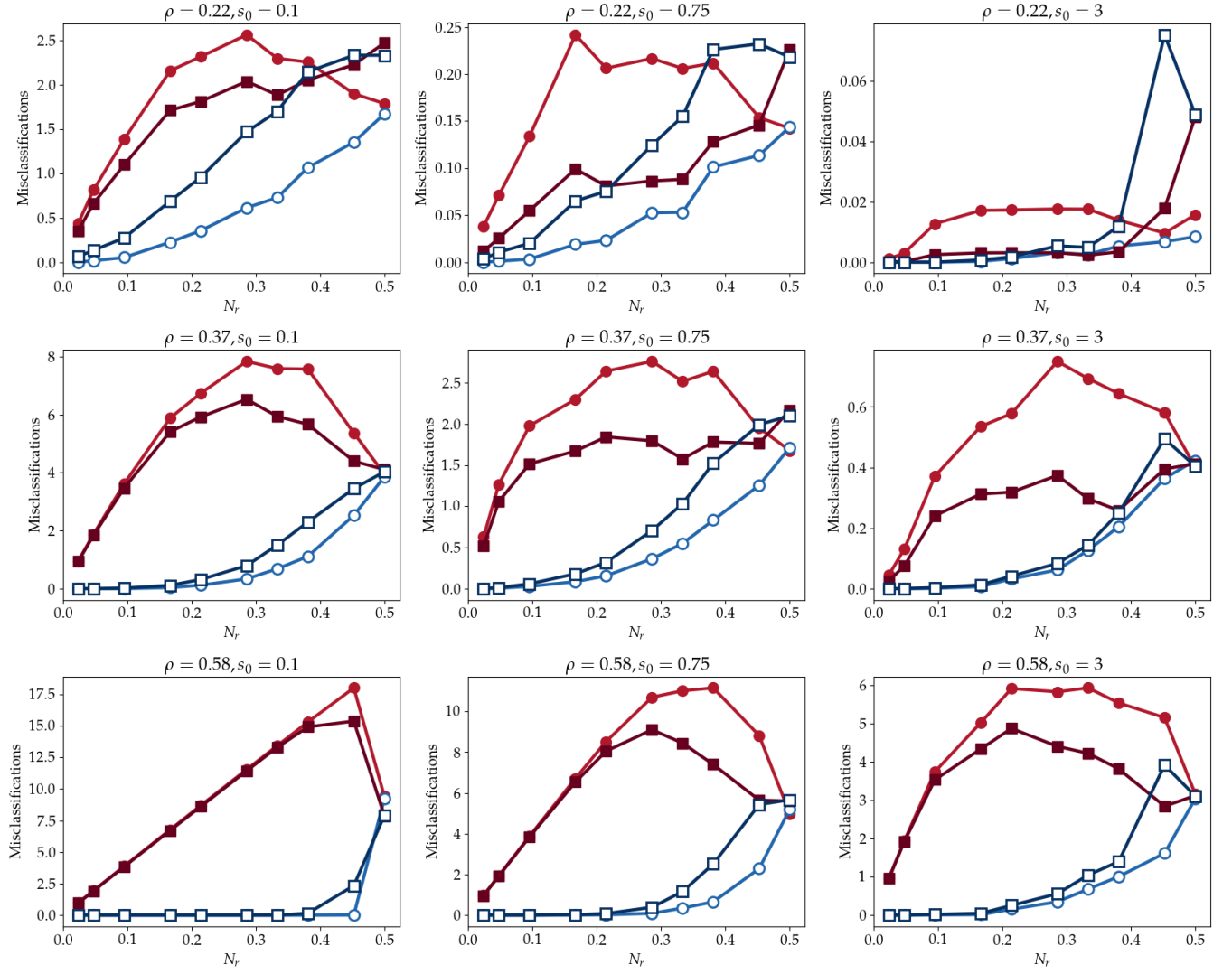


FIG. 5. Number of misclassifications versus N_r for the agent-only observer (light colour, circle markers) and the neighbourhood observer (dark color, square markers) for the smaller (red lines, filled markers) and larger (blue lines, empty markers) groups, for various choices of s_0 and ρ .

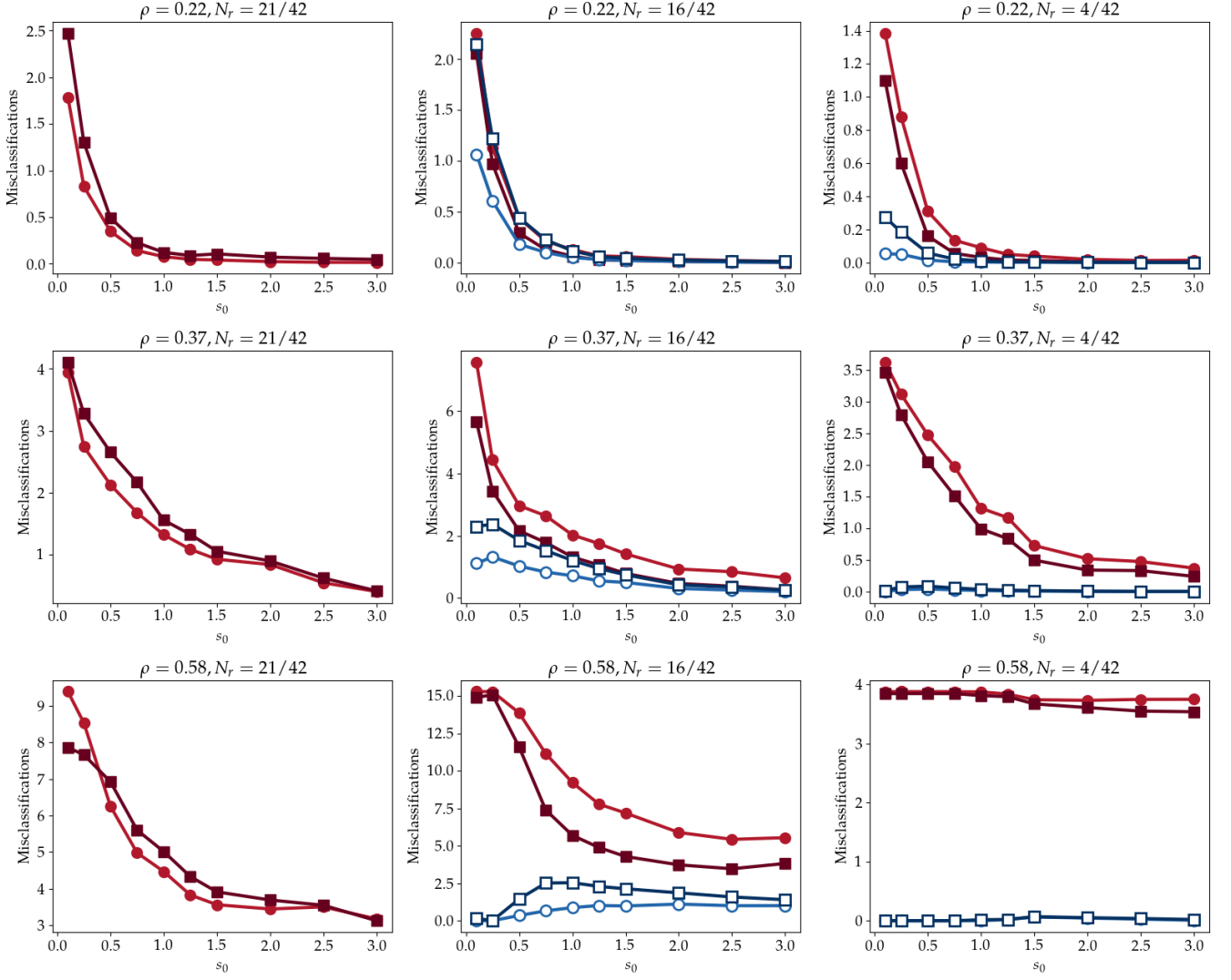


FIG. 6. Number of misclassifications versus s_0 for the two observers. Figure conventions are the same as Figure 5.

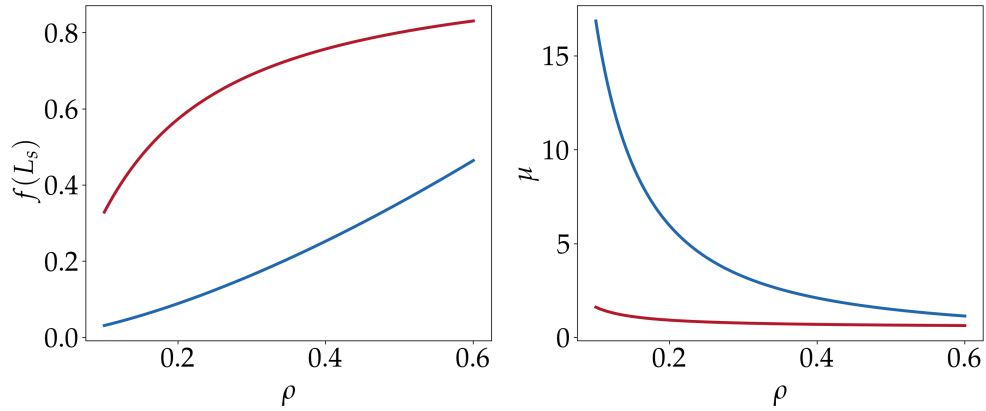


FIG. 7. Left panel: $f(L_s)$ against ρ for $f := f_{\text{poly}}$ (blue) and $f := f_{\text{exp}}$ (red); where $L_s = 1/\sqrt{\rho}$. Left panel: μ against ρ , with μ computed using f_{poly} (blue) and f_{exp} (red). Notice the large variation when μ is computed using f_{poly} .

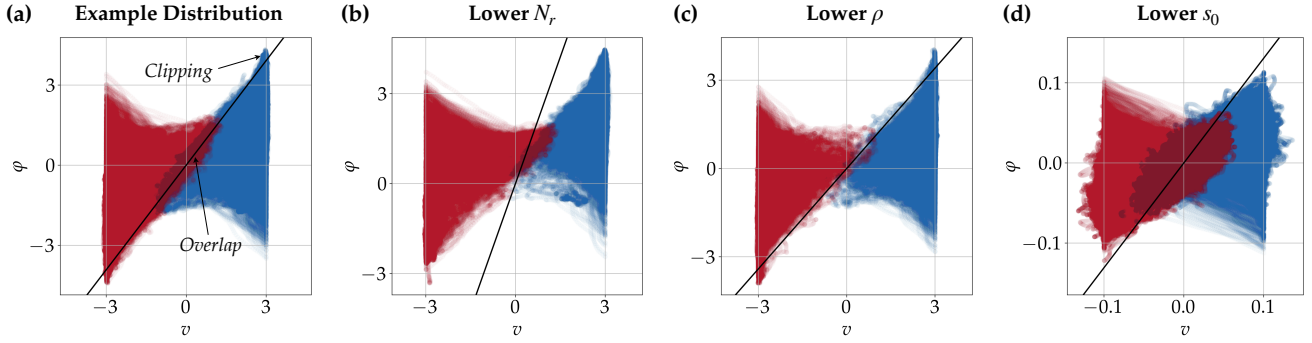


FIG. 8. Joint distribution of v_i^w and φ_i^w , and its dependence on parameters. (a) A typical distribution of agent velocity v_i^w and neighbourhood parameter φ_i^w . $N_r = 1/2, \rho = 0.31, s_0 = 3$. The blue points correspond to agents actually belonging to Group 1, and red points correspond to agents belonging to Group 2. The black line is the classification boundary (of the neighbourhood observer) with slope $1/\mu$. (b) When N_r decreases ($N_r = 1/6$), the distribution of the minority agents (red) shifts upwards, indicating an increase in φ_i^w in the positive direction. The distribution of the majority agents (blue) shifts leftwards and upwards, indicating that fewer agents are being pushed. (c) When ρ decreases ($\rho = 0.22$) the distributions of the two groups move farther apart. (d) When s_0 decreases ($s_0 = 0.1$), all agents are moving very slowly, which also results in low φ_i^w values. There is a large overlap between the distributions of the two groups, making classification difficult.

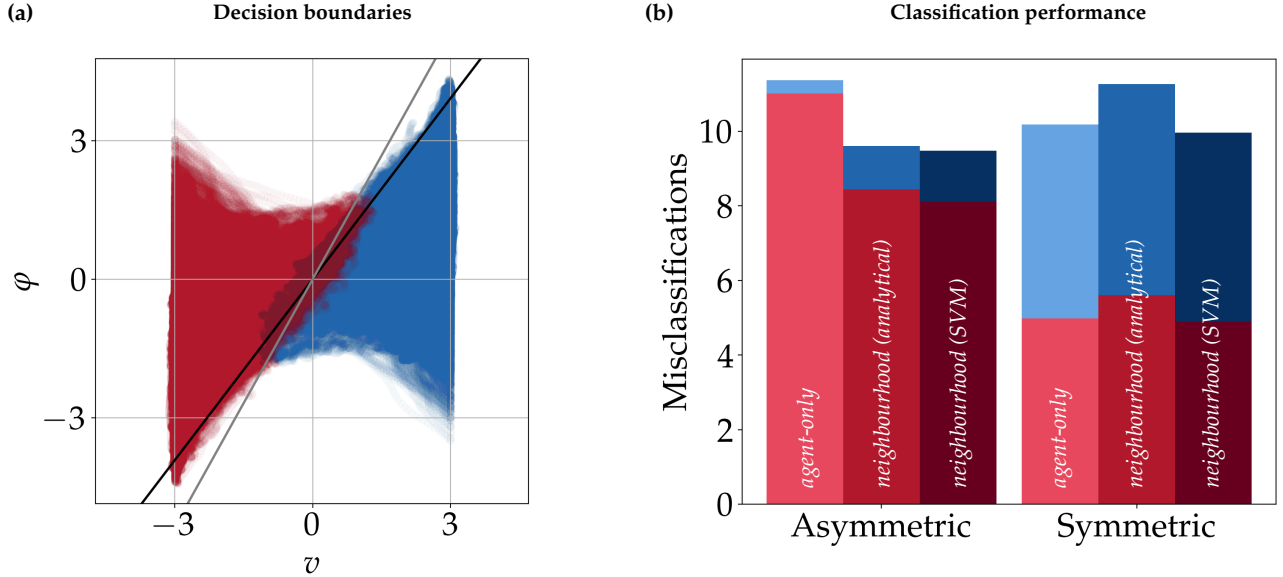


FIG. 9. (a) Comparison between the decision boundaries of the neighbourhood observer and the trained SVM classifier. The black line is the decision boundary of the neighbourhood observer, which is a line through the origin with slope $1/\mu$. The grey line is the decision boundary found by training an SVM. Note how the black line clips the edges of the distributions while the grey line avoids this issue. (b) Comparison of the performances of the 3 classification algorithms: the agent-only observer, the neighbourhood observer (with analytically computed μ) and the trained SVM classifier. The SVM classifier is as good as or better than the neighbourhood observer for asymmetric cases (data shown from $N = 14$). In the symmetric case, the SVM classifier obtains equal or better performance than the agent-only observer, while the neighbourhood observer performs slightly worse.